

Liquid–liquid phase transition in solutions of ionic liquids with halide anions: Criticality and corresponding states*

Annamaria Butka¹, Vlad Romeo Vale¹, Dragos Saracsan¹,
Cornelia Rybarsch¹, Volker C. Weiss², and Wolfram Schröer^{1,‡}

¹*Institute of Inorganic and Physical Chemistry, Fachbereich Biologie-Chemie, University of Bremen, Leobener Strasse NWII, 28359 Bremen, Germany;*

²*Eduard-Zintl-Institute of Inorganic and Physical Chemistry, Technical University of Darmstadt, Petersenstrasse 20, 64287 Darmstadt, Germany*

Abstract: Measurements of the liquid–liquid phase diagrams of solutions of the ionic liquids (ILs) 1-dodecyl-3-methylimidazolium chloride (C₁₂mimCl) in arenes (benzene, toluene, *o*-xylene, tetraline) and 1-tetradecyl-3-methylimidazolium chloride (C₁₄mimCl) in CCl₄ are reported and compared with those of solutions of trihexyl-tetradecyl-phosphonium halides (P_{666 14}Cl, P_{666 14}Br) in hydrocarbons and 1-alkyl-3-methylimidazolium tetrafluoroborates (C_nmimBF₄) in alcohols and water. The phase diagrams of solutions of tetrapentyl-ammonium bromide (N₅₅₅₅Br) in water and KI in SO₂ are also discussed. Except for the KI/SO₂ system, which features a lower critical solution point (LCSP), all systems have an upper critical solution point (UCSP) and show corresponding-states behavior. The experimental data are compared with results from simulations and theory concerning the model fluid of charged hard spheres in a dielectric continuum, termed restricted primitive model (RPM). The analysis in terms of RPM variables shows agreement with the location of the critical point (CP) of the model with noticeable systematic deviations. However, for protic solvents, the CP becomes an LCSP, while in aprotic solvents the CP is a UCSP as expected for Coulomb systems. This indicates that in aprotic solvents, the phase transition is essentially determined by the Coulomb interactions, while in the solutions in protic solvents with hydrogen bonds, both Coulomb and solvophobic interactions are important.

Keywords: ionic liquids; corresponding states; phase diagrams; critical phenomena.

INTRODUCTION

Salts with melting temperatures below 100 °C have been termed ionic liquids (ILs). ILs are organic salts with bulky nonspherical cations. They became a major topic of research in chemistry and chemical engineering because of their potential for many applications [1–3]. There are ILs with melting temperatures as low as 200 K [4]. The vapor pressure of ILs is hardly measurable [5]. Boiling temperatures are expected near 1300 K [6], which is far above the decomposition temperatures near 600 °C [7]. The special properties of molten salts at ambient temperatures suggest applications of ILs as reaction medium,

*Paper based on a presentation at the International Conference on Modern Physical Chemistry for Advanced Materials (MPC '07), 26–30 June 2007, Kharkiv, Ukraine. Other presentations are published in this issue, pp. 1365–1630.

‡Corresponding author: E-mail: schroer@uni-bremen.de

catalyst, and extraction medium, all of which require research on basic physical chemical properties of ILs.

In general, the cations are organic entities with structures that are similar to those of ionic detergents. Thus, the properties of ILs are determined by a complicated interplay of Coulomb interactions and other interactions of the ions. Therefore, the understanding of the macroscopic properties from the microscopic structure provides a formidable challenge for theory and experiments.

For applying ILs in separation processes, a good knowledge of the phase diagrams of the liquid–liquid phase transitions in solutions of ILs is essential. In addition to the aspects of applications, studies of the shape of phase diagrams of solutions of ILs are of fundamental interest: It was hypothesized that the long-range nature of the r^{-1} -Coulomb interactions may change the nature of the critical point (CP) of the phase transition from the universal Ising criticality to some other critical behavior, e.g., to mean-field (mf) criticality [8]. We recall that classical mf theories, such as the van der Waals theory or the regular solution theory, predict a parabolic shape for coexistence curves, while the Ising model predicts a cubic shape. The Ising model is a lattice model that considers occupancy of the lattice by two kinds of particles (spins), where the interactions are described by one interaction parameter only, which makes the interactions between like neighbors energetically favorable, the ones of unlike neighbors unfavorable. Irrespective of the simplicity of the model, it has been shown by experiments that the critical properties of the liquid–gas phase transitions and of the liquid–liquid phase transitions [9] of non-ionic fluids are in accordance with the properties of the Ising model in three dimensions (3D). According to theory, Ising criticality is generally expected if the phase transition is determined by short-range interactions, defined as r^{-n} interactions with $n > 4.97$ [10], which is certainly true for r^{-6} dispersion interactions and angular averaged dipole–dipole interactions.

The interest in the criticality of ionic solutions was triggered by reports of mf critical behavior for the liquid–liquid phase separation in the solution of a salt with a low melting point in an almost non-polar solvent [11,12]. However, later measurements showed that the liquid–liquid phase transition of this particular system [13] and of other ionic solutions belong to the Ising universality class [14]. This is in agreement with simulation results on the simplest model for an ionic fluid, the restricted primitive model (RPM), which considers a system of charged hard spheres of equal size in a dielectric continuum with the dielectric constant ϵ [15–19]. According to the correspondence principle [9], the critical properties of the liquid–gas phase transition of this model are expected to apply also for the liquid–liquid phase transition, where the dielectric constant may be identified with that of the solvent. Applying finite-size scaling technique simulations (fss sim) of the RPM [15–19] and of generalizations, which allow for different sizes and charges [20,21] of the ions, yields Ising critical behavior. Simulations on this level are restricted to very simple models such as the RPM or the Lennard–Jones fluid. Simulations of realistic models, which allow predictions of critical properties of real ionic solutions, are not possible at present.

Thus, simulations and experiments support the conclusion that it is now almost certain that the liquid–liquid phase transition in ionic systems belongs to the Ising-universality class [22]. Nevertheless, some uncertainty remains. Experimental deficiencies may easily lead to erroneous conclusions [23]; chemical instability of the salts considered in the older work is an issue of concern. Therefore, experiments on solutions with the new ILs can be expected to provide a definite answer. Furthermore, there are subtle critical phenomena, such as the cross-over from Ising to mf criticality [24] and the curvature of the diameter [25,26], that are due to be investigated in detail. The large number of ILs, which are now commercially available in good quality, suggest systematic studies on the liquid–liquid phase transition of ILs in solutions in order to shed light on the relations of molecular interactions to thermodynamic properties.

The concept of corresponding states has proved to be a powerful tool in order to reduce the data and also to pinpoint general aspects of the systems under consideration. The theorem of corresponding states, which goes back to van der Waals, predicts that scaling the thermodynamic variables in terms of their critical values leads to a universal representation of the thermodynamic properties (e.g., of the

phase diagrams). The phase diagrams match on a master curve when represented in terms of variables scaled in such a manner. Later on, it was proven by statistical thermodynamics that the theorem of corresponding states rigorously applies if the intermolecular potential is of the form $u = u_0 \cdot \varphi(\sigma/r)$, where u_0 and σ are parameters of the energy and of the separation [27]. The Lennard–Jones potential $u_{\text{LJ}} = u_0 \cdot [(\sigma/r)^{12} - (\sigma/r)^6]$ is an example of such a potential. Then a reduced temperature $T^* = kT/u_0$ and a reduced density $\rho^* = \rho \cdot \sigma^3$ may be defined, allowing for a presentation of all thermodynamic properties in terms of the reduced variables. Furthermore, in terms of the reduced variables, the critical data T_c^* and ρ_c^* are independent of the particular values of u_0 and σ provided $\varphi(\sigma/r)$ is of the same form. Guggenheim's analysis of the phase diagrams of the liquid–gas phase transition of simple compounds [28] demonstrated not only the validity of the corresponding-states approach for typical fluids, but showed the failure of the conventional mf theories that predict a parabolic shape for the phase diagrams, while experiments prove a cubic shape in agreement with the predictions of the Ising model.

As outlined above, the theorem of corresponding states can rigorously apply only to such groups of compounds that may be described by a two-parameter potential of the same mathematical form. Nevertheless, approximate validity is found more frequently. Otherwise, as emphasized by Guggenheim [28], the deviations from the corresponding-states behavior give valuable hints on specific properties of groups of systems, which may not be seen in an analysis in terms of common thermodynamic variables [29].

Considering ionic solutions, the RPM is a useful guide for the corresponding-states analysis of the phase diagrams of ionic systems because critical data and critical properties are known from simulations for this model [15–19]. With an estimate of the ion–ion distance σ in the ion pair and the knowledge of the dielectric permittivity ε of the solvent, the experimental data can be expressed in terms of the reduced variables

$$T^* = \frac{kT \cdot \varepsilon \cdot \sigma}{q^2} \text{ and } \rho^* = \rho \cdot \sigma^3 \quad (1)$$

of this model, where q is the charge of the ions and ρ the number density of the ions. This approach has successfully been applied for finding liquid–liquid phase transitions in ionic solutions [30]. For solutions in nonpolar solvents, the critical temperatures in RPM variables have been found to agree reasonably well with the figures obtained by simulation of this model [31]. However, analyzing the experimental data for polar solvents, it is observed that, in variance to the prediction of the RPM, the reduced critical temperatures depend almost linearly on the dielectric permittivity of the solvent [32–34]. This observation indicates a continuous change from phase transitions driven by Coulomb interactions in nonpolar solvents to a mechanism based on solvophobic interactions in solvents of high dielectric constant.

In this work, we continue our systematic study of the phase diagrams of binary solutions of ILs. The phase diagrams are analyzed in order to display general properties and regularities. Most work reported in the literature concerns solutions in alcohols [32–38]. Reports on liquid–liquid demixing in nonpolar and aprotic solvents are rare [39–42]. We present a systematic study of the phase diagrams of binary solutions of ILs with a halide anion in aprotic solvents. We compare the properties of solutions in protic and aprotic solvents. The nonpolar solvents considered here are alkanes (heptane, octane, nonane, decane), arenes (benzene, toluene, *o*-xylene, tetraline), and CCl_4 . Data on solutions in alcohols and water are discussed. We include the historical work of Walden and Centnerszwer on KI in SO_2 [43] in the discussion and analyze it within the framework of the theory of critical phenomena and of the theorem of corresponding states together with the solutions of the ILs.

METHODOLOGY

Data analysis of phase diagrams

Presuming Ising criticality, the temperature dependence of a concentration variable X at coexistence near the CP can be represented by a power series [9,44] in $\tau = |T - T_c|/T_c$, termed Wegner expansion, which is of the form

$$\frac{X_{\pm}}{X_c} = \frac{X_m}{X_c} \pm B \cdot \tau^{\beta} \left(1 + B_1 \cdot \tau^{\Delta} + B_2 \cdot \tau^{2\Delta} + \dots \right) \quad (2)$$

where

$$\frac{X_m}{X_c} = 1 + A \cdot \tau + C \cdot \tau^{2\beta} + D \cdot \tau^{1-\alpha} \left(1 + D_1 \tau^{\Delta} + \dots \right) \quad (3)$$

By X , we denote a variable for the composition that will be discussed below. The plus refers to the region $X > X_m$ and vice versa; X_m is the so-called diameter, defined by the average $X_m = (X_+ + X_-)/2$ of the compositions X_+ and X_- of the coexisting phases. For the Ising model, the exponents assume the universal values $\beta = 0.325$, $\alpha = 0.11$, and $\Delta = 0.51$, where β is the leading exponent for the phase diagram, α is the exponent of the heat capacity, and Δ is the cross-over exponent, describing the cross-over from Ising to classical mf behavior. In mf theories $\beta = 1/2$ and $\alpha = 0$, so that the rectilinear diameter rule of Cailletet–Mathias, which assumes a linear temperature dependence of the diameter, applies in mf theory. By definition, there is no cross-over exponent Δ in mf models. While the exponents are universal, the amplitudes are specific for the system. The corrections to scaling that are given in eqs. 2 and 3 suffice in the region $\tau < 10^{-2}$ [9]. In general, a cross-over theory [24] should be applied when analyzing data in a wider temperature region. At large distance from the CP, other specific contributions become important and universality loses applicability.

The temperature dependence of the diameter has long been a matter of controversy [45,46]. For a long time it had been accepted that the $(1-\alpha)$ -term is the leading term near the CP, while the 2β -term was regarded as the consequence of a nonappropriate choice of the concentration variable. Recent theoretical work, termed “complete scaling”, advocates the number density as the appropriate variable [47] and suggests the 2β -term as the leading part [25,26,48]. However, partial cancellation of the 2β - and the $(1-\alpha)$ -terms may cause apparent linear temperature dependence of the diameter [25]. Thus, deviations from the linear temperature dependence are often small. Therefore, it is difficult to determine uniquely the various coefficients of eq. 3 by a numerical analysis, even of the best experimental data. Notably, simulations of the RPM have not reached the accuracy to show the nonanalytical contributions to the diameter of the phase diagram.

The analysis of phase diagrams using eqs. 2 and 3 or the more advanced theories requires precise knowledge of the data of the CP and measurements with mK-accuracy. Most phase diagrams reported in the literature are obtained by the so-called visual method, where the temperature of the cloud point for samples of different composition is measured. This method, which is also used in this work, is mostly not accurate enough to allow for a data analysis by eqs. 2 and 3, but suffices to locate the CPs and to find general aspects of the phase diagrams. In fact, the work presented here is a screening work in order to find systems suitable for more involved investigations of critical phenomena. Therefore, it is sufficient to apply a simpler approach for the data evaluation here.

In the engineering literature, classical expansions are commonly used for estimation and fitting excess functions, which implies mf exponents for the critical properties, e.g., for the shape of the coexistence curve [49]. By this approach, the fundamental fact that the liquid–liquid phase transition belongs to the Ising universality class is ignored. Therefore, we apply a method [31,34], which is simpler than eqs. 2 and 3 but takes care of the nonclassical nature of the phase diagrams. The simplified scaling laws applied in the analysis are

$$X_{\pm} - X_m = \pm b \cdot (T_c - T)^{1/3} \quad (4)$$

where

$$X_m = X_c + a \cdot (T_c - T) \quad (5)$$

The lower-case letters a and b in eqs. 4 and 5 indicate that we do not use scaled variables such as $\tau = |T - T_c|/T_c$. Equations 4 and 5 lead to a cubic equation for T , which can be solved exactly. However, the resulting solutions are too messy to be applied in a fitting procedure. In many cases, the slope of the diameter is not very large and an expansion of $|X - X_m|^3$ in first order of a suffices. The resulting function $T(X)$, which will be used as fitting function, is

$$T = T_c - \frac{|X - X_c|^3}{b^3 \pm 3a \cdot (X - X_c)^2} \quad (6)$$

The positive and negative signs correspond to the range $X < X_c$ and $X > X_c$, respectively. For a lower critical solution point (LCSP), the sign in front of the fraction becomes positive. Alternatively, the signs of b and a may be changed for describing phase diagrams with a lower solution point. The parameters of the fit are the critical data T_c , X_c , the width b of the coexistence curve and the slope a of the diameter. By such a fit the nonclassical shape of the phase diagrams is taken into account in reasonable approximation. The approximation $\beta = 1/3$, which was also used by Guggenheim, is near to the Ising value $\beta = 0.325$ and suffices for our purpose. Note that straightforward fits by an analytic power series not only imply classical exponents, but often also lead to erroneous descriptions, e.g., by showing spurious maxima. In mf theory, the equations corresponding to eqs. 4 and 5 are quadratic equations with a simple exact solution. In an equation analogous to eq. 6, the powers of b and $(X - X_c)$ are reduced by one and the factor three in the denominator is replaced by the factor two. Equation 6 may also be applied for fitting corresponding-states diagrams in terms of the variables $\Delta X = |X - X_c|/X_c$ and $\tau = |T - T_c|/T_c$. The fit parameters are then termed A and B because they are approximations to the coefficients in eqs. 2 and 3.

On experimental grounds, many choices for the composition variable X can be thought of, e.g., the mole fraction x , the mass fraction w , the volume fraction φ , or the number densities ρ_i of the components. The mass fraction is most directly related to the experiment. From the physical point of view, however, w is not appropriate because the masses are irrelevant for the thermodynamics of fluids. We report the data in terms of the mole fraction, which is obtained from the mass fraction without approximation. We also analyze the data in terms of the reduced ion number density of the salt, which is the variable used in theories and simulations of the RPM. The number density should generally be used when investigating liquid–liquid phase transitions that are well separated from a liquid–gas transition [47]. The application of the partial density as variable, however, requires the knowledge of the density as function of temperature and concentration. In good approximation, the densities can be estimated by assuming additive molar volumes, thus ignoring the excess volumes. In this approximation, the reduced ion number density ρ^* , which is the corresponding-states variable of the RPM, is estimated from the mole fraction x_{IL} of the IL and the molar volumes V_{IL} and V_{S} of the ILs and of the solvents.

$$\rho^* = \frac{2 \cdot x_{\text{IL}} \cdot \sigma^3 \cdot N_{\text{A}}}{x_{\text{IL}} \cdot V_{\text{IL}} + (1 - x_{\text{IL}}) \cdot V_{\text{S}}} \quad (7)$$

N_{A} is Avogadro's number. In the RPM, σ is the ion diameter which is identical with the charge separation. In the analysis of the experimental phase diagrams, we take the distance of the centers of the distributed charges of the ions at contact as the distance σ . With this choice, we adapt the RPM variables, given in eqs. 1 and 7, for the analysis of real ionic solutions.

Theoretical predictions for the phase diagrams

A complete theory which treats the nonclassical singularities at the CP of ionic fluids adequately and which predicts the coefficients in eqs. 2 and 3 correctly is not available. This is true even for the RPM. Thus, we can only compare our experimental findings with the results of fits to simulation data for this model [15–19]. At the mean-field level, however, there are quite successful theories which compare well with the results of earlier simulations [50–52] that did not use fss techniques and may be regarded as "mean-field" simulations. In Fig. 1, we show the phase diagrams obtained by different methods for the RPM. The open squares are simulation data taken from ref. [50]. The filled squares are the simulation results of ref. [19] obtained by using fss techniques. The dashed curve is the fit to the simulation data using eq. 5 for the analysis. The continuous curve is the result of the analytical theory of Fisher–Levin (FL) [53,54] that we will discuss here.

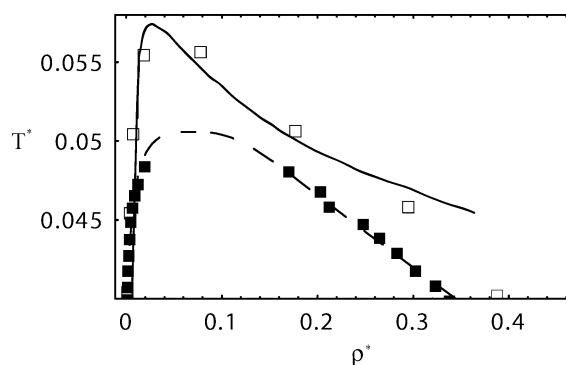


Fig. 1 Phase diagrams of the RPM. The continuous line is the prediction of the FL theory, The squares are simulation results applying (filled square) [19] and not applying (open square) [50] fss techniques. The dotted line is the fit using eq. 6.

One of the simplest of these theories for the RPM is the Debye–Hückel (DH) theory [55], which accounts for electrostatic interactions among the ions. An extension of this early theory of ionic fluids was developed by Fisher and Levin [53,54]; their refined theory predicts a coexistence curve which agrees quite well with the results of early simulations [50–52] that did not use the finite-size scaling techniques applied in later simulations [15–19]. The FL theory goes beyond the original DH theory for strong electrolytes by incorporating ion pairing (following the ideas of Bjerrum) and accounting for the interactions of free ions and ion pairs at the same level as DH theory does for ion–ion interactions. The RPM is a one-component system, and the theory thus yields an upper CP. The predictions obtained from the FL theory for the critical data of the RPM are close to those found in the above-mentioned "mean-field" simulations. According to the nature of mean-field theories, the critical temperature is overestimated if compared to the results of simulations in which proper finite-size scaling is employed. Nevertheless, the critical data are located in the correct region of the temperature-density plane by the FL theory; the DH theory is quite successful for the critical temperature, but largely (by an order of magnitude) underestimates the critical density.

An advantage of analytical theories, as compared to simulations, is that they provide a complete solution for the thermodynamic space and not just the result for one particular point. Explicit expressions for the free energy density can be obtained, which, close to the CP, can be written as a power series (double Taylor expansion) in terms of the corresponding-state variables $\Delta\rho^* = |\rho^* - \rho_c^*|/\rho_c^*$ and $\tau^* = |T^* - T_c^*|/T_c^*$. The coefficients in this expansion, known as the Landau expansion, can be calculated from the theory. We denote these coefficients by c_{ij} , where the first index means the i^{th} derivative with respect to $\Delta\rho^*$ and the second index is the j^{th} derivative with respect to τ^* , evaluated at the CP [56].

Such theories allow us to obtain asymptotic expressions for the width of the coexistence curve B^* and the slope of the diameter of the coexistence curve, A^* [56]:

$$B^* = \left(\frac{6c_{21}}{c_{40}} \right)^{1/2} \quad \text{and} \quad A^* = \frac{c_{31}}{c_{40}} - \frac{3c_{21}c_{50}}{5c_{40}^2} \quad (8)$$

The star indicates that RPM variables are used for calculating the corresponding-state variables τ^* and $\Delta\rho^*$. Note that in the RPM the corresponding-states variables τ^* and $\Delta\rho^*$ are identical to the conventional corresponding-states variables τ and $\Delta\rho$ because the molecular parameters, defining T^* and ρ^* in eq. 2, are constant and cancel in the corresponding-states variables.

The results for the critical parameters T_c^* , ρ_c^* , and the quantities A^* and B^* are compiled in Table 1 for either mean-field theory for the RPM that we consider here. For comparison, we include the results of our fits using eq. 6 to the data of the “mean-field” simulation (mf sim) and to the simulation using fss sim.

Table 1 Critical parameters of the RPM in theory and simulation: The table gives the coordinates of the CPs T_c^* and ρ_c^* , the asymptotic widths of the coexistence curves B^* and asymptotic slopes of the diameter of the coexistence curves A^* for the DH theory, the FL theory, and the results of the fits to the data of the early mean-field simulation (mf sim) and a recent simulation using finite-size scaling techniques (fss sim).

Theory	T_c^*	ρ_c^*	B^*	A^*
DH	0.0625	0.00497	6.93	19.8
FL	0.0574	0.02778	3.87	11.6
mf sim [50]	0.0566	0.0447	5.01	11.4
fss sim [19]	0.0506	0.0696	2.78	5.83

Experimental details

The ILs 1-dodecyl-3-methylimidazolium chloride ($C_{12}\text{mimCl}$) and 1-tetradecyl-3-methylimidazolium chloride ($C_{14}\text{mimCl}$) were purchased from Merck. The purities certified by the producer were >98 %. Standard NMR and MS analysis did not show impurities. The solvents were chosen of highest quality. Using a glove box under Argon atmosphere, the ILs were filled into a glass sample cell using a syringe and then dried for 30 h at 60 °C under vacuum of $6 \cdot 10^{-3}$ bar. Traces of water were removed from the solvents by adding P_2O_5 . The “pump and freeze” technique at the vacuum line was used to remove the gases and volatile compounds from the solvents and from the ILs. The solvent was condensed via the vacuum line into the sample cell that was cooled with liquid nitrogen. A Teflon tap (Normag) attached to the sample cell enabled connecting and removing the sample cell from the vacuum line, thus allowing us to weigh the sample during the drying process, and also when changing the solvent content. The concentrations were determined by weight with an accuracy of 10^{-4} g. In this manner, a set of concentrations is prepared by adding or removing solvent from the sample by distillation on the vacuum line with the identical sample of the IL. Using this method, the amount of the IL is constant. Uncontrollable traces of impurities that could cause deformations of the separation curves, when different samples are investigated, are avoided. Mixtures with the mass fractions ranging from 0.03 to 0.27 were prepared in this way.

The cloud points were determined visually by repeated cooling of the homogeneous mixture in a thermostat with glass windows filled with water. The cloud points have been measured in a temperature region of 10 K below the CP for 5–10 different concentrations. The temperature was controlled with an

accuracy of 0.01 °C using a Quartz thermometer (Heraeus QUAT200). The temperature range investigated reached from 16 to 90 °C. Measurements at higher temperatures were carried out in a bath of silicon oil. Clearly, the accuracy of the visual method is limited by the subjectivity of the experimentalist. The visual method is appropriate to get an overview and the first step for the preparation of samples of critical composition.

RESULTS

Phase diagrams using the mole fraction as composition variable

In Fig. 2, we show the phase diagrams for various ionic solutions with halide anions as function of the mole fraction calculated from the weight fraction of the samples.

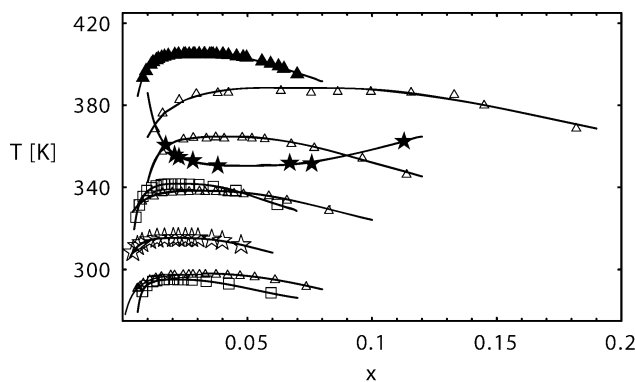


Fig. 2 Phase diagrams of ionic solutions with halide anions in aprotic solvents with the mole fraction x of the IL as concentration variable. The figure shows the separation temperatures of the solutions of $C_{12}\text{mimCl}$ in benzene, toluene, *o*-xylene, tetraline, (Δ) (bottom to top), $C_{14}\text{mimCl}$ in CCl_4 (\star), $\text{P}_{666\ 14}\text{Cl}$ and $\text{P}_{666\ 14}\text{Br}$ (bottom to top) in heptane (\square) [31], N_{5555}Br in water (\blacktriangle) [57], and KI in SO_2 (\star) [43]. The lines are fits with eq. 6.

The separation temperatures of the solutions of $C_{12}\text{mimCl}$ in benzene, toluene, *o*-xylene, and tetraline increase in this order. The separation temperatures of the solutions of $C_{14}\text{mimCl}$ in CCl_4 are between those of benzene and toluene. In the solutions of $\text{P}_{666\ 14}\text{Cl}$ and $\text{P}_{666\ 14}\text{Br}$ in heptane [31], the bromide has the higher separation temperature. We have included the data of Japas and Levelt Sengers concerning the solution of tetrapentyl ammonium bromide (N_{5555}Br) in water [57] and the data of the historical measurement of Walden and Centnerzwer on the solution of KI in SO_2 [43]. With the exception of the KI/SO_2 solutions with an LCSP, all systems have an upper critical solution point (UCSP). All critical mole fractions are at small mole fractions below 0.1. The curves are the fits using eq. 5. Within the accuracy of the measurements, the quality of the fits is perfect.

The fit parameters are given in Table 2. The table lists the critical temperatures, the critical mole fractions, the widths b , and the asymmetry parameters a of the coexistence curve. The table includes the data for the systems $\text{P}_{666\ 14}\text{Cl}$ and $\text{P}_{666\ 14}\text{Br}$ in heptane [31] and some data of the solutions of $C_6\text{mimBF}_4$ in H_2O and *n*-alcohols [32] (in the short-hand notation $C_n\text{OH}$ indicating the chain length of the alcohols). The critical compositions for the ILs with the halide anion are rather low, between 0.02 and 0.1. For the alcohol solutions, the figures for x_c , a , and b are slightly larger than for the solutions with aprotic solvents. The statistical uncertainties given by the fits are $\Delta T_c = 0.02\ \text{K}$ for the temperature and below 5 % for the other parameters. We recall that the fit assuming the rectilinear diameter is only an approximation, which, nevertheless, is appropriate in view of the accuracy of the measurements. Due to the neglect of the nonanalytic behavior of the diameter, the estimates of the critical compositions may

be expected to be slightly too high. In any case, the estimates of the critical compositions are rather good starting values for the more involved experiments determining the critical composition according to the equal volume criteria.

Table 2 Parameters of the phase diagrams of ionic solutions with the mole fraction x as concentration variable. The parameters b , a concern the fits by eq. 6 to the original data (Fig. 2), while A and B are the parameters of the corresponding-states plots (Fig. 3).

System	T_c/K	x_c	$b/K^{-1/3}$	a/K^{-1}	B	A
$C_6\text{mimBF}_4\text{-H}_2\text{O}$	330.98	0.041	0.0274	0.0054	4.67	29.58
$C_6\text{mimBF}_4\text{-C}_3\text{OH}$	287.71	0.102	0.0673	0.0098	4.37	27.76
$C_6\text{mimBF}_4\text{-C}_6\text{OH}$	326.41	0.149	0.0897	0.0083	4.14	18.22
$P_{666\ 14}\text{ Cl-heptane}$	295.13	0.023	0.0116	0.0015	3.40	19.76
$P_{666\ 14}\text{ Br-heptane}$	341.73	0.025	0.0112	0.0009	3.18	12.84
$C_{12}\text{mimCl-benzene}$	297.45	0.032	0.0175	0.0013	3.65	12.28
$C_{12}\text{mimCl-toluene}$	337.76	0.032	0.0172	0.0012	3.73	13.05
$C_{12}\text{mimCl-}o\text{-xylene}$	364.25	0.041	0.0167	0.0011	2.87	9.63
$C_{12}\text{mimCl-}o\text{-tetraline}$	388.02	0.071	0.0292	0.0014	3.02	7.84
$C_{14}\text{mimCl-CCl}_4$	315.40	0.023	0.013	0.0012	3.89	16.35
$N_{5555}\text{Br-H}_2\text{O}$	405.04	0.031	0.013	0.0009	3.23	12.17
KI-SO_2	350.62	0.050	0.020	0.0012	2.74	8.08

As the next step, we investigate the corresponding-states behavior. In Fig. 3, we show the reduced temperature $(T - T_c)/T_c$ as a function of $(x - x_c)/x_c$ for the systems under consideration. The symbols have the same meaning as those used in Fig. 2. We have included the data points of the solutions of $C_n\text{mimBF}_4$ in alcohols and water (open diamond). The figure includes the data for the solutions of $C_4\text{mimBF}_4$ in alcohols ($C_n\text{OH}$, $n = 3, 4, 6, 8$) [34,37] and $C_6\text{mimBF}_4$ in alcohols ($C_n\text{OH}$, $n = 3, 4, 5, 6$) [32,34]. We find wide agreement among the various data sets with the obvious deviation for the KI SO_2 system showing an LCSP. Widths and asymmetries of the solutions in the alcohols are bigger than for the ionic solutions in aprotic solvents. The lines connecting the systems KI/SO_2 and $N_{5555}\text{Br}/\text{H}_2\text{O}$ are calculated with the fit parameters B and A , also given in Table 2. The fits are obtained with eq. 6 but applying the reduced variables. For the solutions in the aprotic solvents, the width B varies between 2.7 and 3.9. In this representation, the slope of the diameter A is larger than B with a rather large variation

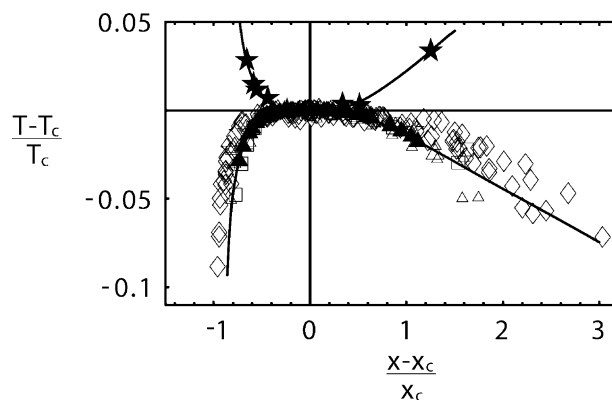


Fig. 3 Corresponding-states phase diagram with the mole fraction as concentration variable. The meaning of the symbols is the same as in Fig. 2. The solutions of $C_n\text{mimBF}_4$ in alcohols and water are represented by open diamonds. The lines are fits by eq. 6 for the systems KI/SO_2 with an LCSP and $N_{5555}\text{Br}/\text{H}_2\text{O}$.

between 7 and 22. The data in Table 2 state the larger figures of the widths and of the asymmetries of the solutions in the alcohols if compared with the ionic solutions in aprotic solvents.

Phase diagrams in terms of the RPM variables

The RPM has proved to be a useful guide in the search for phase transitions driven by Coulomb forces [22,30]. If the phase transition is driven by Coulomb interactions, it can be expected that the CP is located in the region predicted by the RPM if the appropriate RPM variables, defined in eqs. 1 and 7, are used. Using these variables, a comparison of the experimental phase diagrams with the one obtained from simulations of the RPM is possible and will be carried out in this subsection.

For this purpose, the experimental variables T and x have to be transformed into the RPM variables. For estimating the partial densities, we need the mass densities of the ILs and of the solvents. For estimating the mass densities of the imidazolium ILs, we use the increments given by Esperanca et al. [58] for the molar volumes at normal conditions yielding 0.9661 and 0.9505 g/cm³ for C₁₂mimCl and C₁₄mimCl, respectively, and assume a linear temperature variation of the densities of -10^{-3} g/(cm³ K), which is in the region found for other ILs [59]. The mass densities of the phosphonium ILs are taken from the figures given in ref. [60], fitted by a linear relation. For KI, the crystal density $d = 3.13$ g/cm³ is used [61]. The mass densities of the alkanes are taken from ref. [62]. For SO₂, we assume the density at coexistence at the given temperature [63]. For calculating the RPM temperatures, we use the dielectric permittivities of the solvents given in ref. [64], which are fitted by a power law.

The separation σ is estimated using X-ray results. For KI, we take 3.53 Å [65]. For the imidazolium salts, the center of charge is assumed to be located at the center of the imidazolium ring; the corresponding distance to the chloride ion in C₁mimCl is 3.79 Å [32,66], which is near the figure found in neutron-scattering investigations of the melt [67]. For the C_{*n*}mim BF₄ ILs, we replace the van der Waals radius of the chloride ion (1.81 Å) by an estimate of the van der Waals radius of the BF₄ ion obtained by summing the length of the BF bond (1.4 Å) [65] and the van der Waals radius of a bound fluorine atom (1.35 Å) [61]. The figures for σ of P_{666 14}Cl (4.75 Å), P_{666 14} Br (4.86 Å), and N₅₅₅₅ Br (4.74 Å) are estimated [31] by interpolating results of an X-ray investigation [68] of crystals of symmetric phosphonium and ammonium salts of comparable size.

In Fig. 4, we see the phase diagram drawn with the RPM density as composition variable. Remarkably, the phase diagram of N₅₅₅₅Br in water is centered now at a much higher density than the phase diagrams of the solutions in hydrocarbons. The KI/SO₂ phase diagram has its minimum between

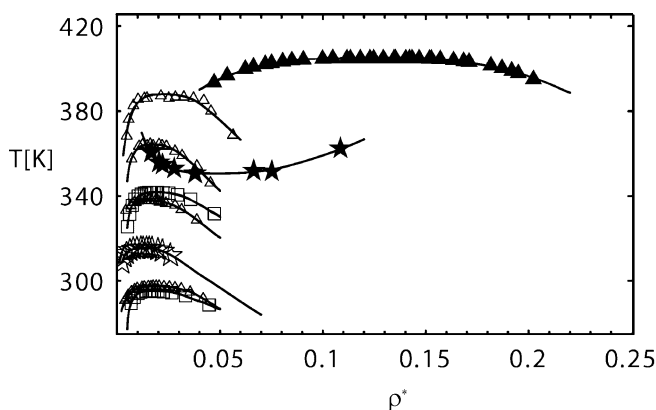


Fig. 4 Phase diagrams of ionic solutions with halide anions in aprotic solvents with the RPM density as concentration variable. Symbols have the same meaning as in Fig. 2.

those two cases. The corresponding-states diagram looks similar to that shown in Fig. 3 and, therefore, is not shown.

In Fig. 5, we now show the phase diagrams in terms of the RPM variables T^* and ρ^* . Symbols have the same meaning as in Figs. 2 and 3. The dashed line is the coexistence curve of the RPM shown in Fig. 1. The difference in the critical temperature of the RPM estimated by the classical FL theory and the simulations employing fss techniques could hardly be seen on this scale. The parameters of the fits are given in Table 3. Note that in the RPM the dielectric constant is regarded as a constant, while in reality the dielectric constant of a solvent depends on temperature. This is taken into account when estimating the RPM temperatures of the phase transition. In former work [31–34], the value of ϵ in a phase diagram was fixed to the figure at T_c of the system considered. Remarkably, the separation temperatures of the manifold of solutions in hydrocarbons virtually collapse to one line, which is

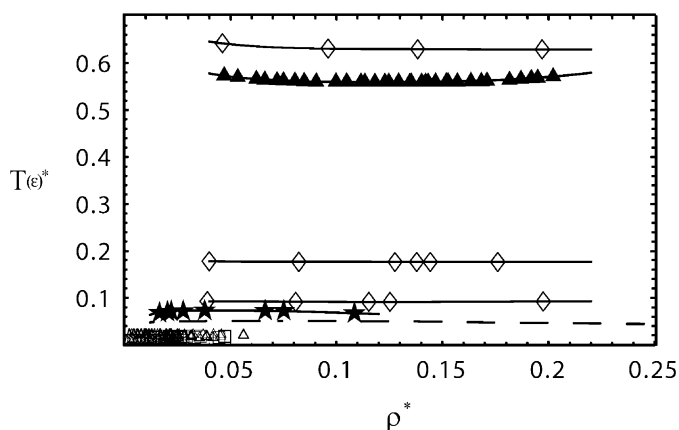


Fig. 5 Phase diagrams of ionic solutions with halide anions in aprotic solvents with the RPM density as concentration variable. Symbols have the same meaning as in previous figures. The dashed line is the phase diagram of the RPM. The open diamonds represent the phase diagrams of $C_6\text{mimBF}_4$ in hexanol, propanol, and water.

Table 3 Parameters of the phase diagrams of ionic solutions in RPM variables. The parameters b^* and a^* concern the fits by eq. 7 to the data rescaled according eq. 1. A^* and B^* are the parameters of the corresponding-states plots (Fig. 7).

System	T_c^*	ρ_c^*	b^*	a^*	B^*	A^*	ϵ_c
$C_6\text{mimBF}_4\text{-H}_2\text{O}$	0.629	0.188	0.792	4.66	3.61	15.59	67.30
$C_6\text{mimBF}_4\text{-C}_3\text{OH}$	0.177	0.136	0.939	11.23	3.87	14.54	21.75
$C_6\text{mimBF}_4\text{-C}_6\text{OH}$	0.091	0.126	0.932	10.02	3.32	7.21	9.84
$P_{666\ 14}\ \text{Cl-heptane}$	0.0163	0.019	0.252	23.64	3.46	20.84	1.92
$P_{666\ 14}\ \text{Br-heptane}$	0.0186	0.020	0.249	15.79	3.31	14.73	1.85
$C_{12}\text{mimCl-benzene}$	0.015	0.019	0.299	16.09	3.79	12.42	2.28
$C_{12}\text{mimCl-toluene}$	0.017	0.016	0.257	15.40	4.15	16.44	2.27
$C_{12}\text{mimCl-}o\text{-xylene}$	0.019	0.018	0.228	13.98	3.40	14.77	2.34
$C_{12}\text{mimCl-}o\text{-tetraline}$	0.021	0.023	0.289	12.40	3.46	11.40	2.48
$C_{14}\text{mimCl-CCl}_4$	0.015	0.013	0.217	16.51	4.19	19.69	2.19
$N_{5555}\text{Br-H}_2\text{O}$	0.56	0.124	0.339	0.26	2.26	1.17	48.16
KI-SO_2	0.073	0.050	0.243	2.03	2.04	3.00	9.78
<i>RPM</i>	0.051	0.070	0.524	8.03	2.78	5.63	(1.00)

below the RPM curve. The separation curve for KI/SO₂ is slightly above, but very near the RPM phase diagram. Again, we have included the data (open diamond) for C₆mimBF₄ in hexanol, propanol, and water, for which the RPM separation temperature increases in this order. The phase transition of C₆mimBF₄/H₂O is at lower temperature than that of N₅₅₅₅Br/H₂O (measured at elevated pressure) but appears at a higher RPM temperature because of the temperature dependence of the dielectric constant of water.

In order to gain more insight, we look for correlations between the parameters of the fits. In Figs. 6a and 6b, we show the critical temperatures T_c^* and critical densities ρ_c^* of the various ionic solutions in the RPM scale as functions of the dielectric permittivity ϵ_c of the solvent at the CP and compare with the fit-results to the data of the simulation of the RPM and the corresponding predictions of the FL theory.

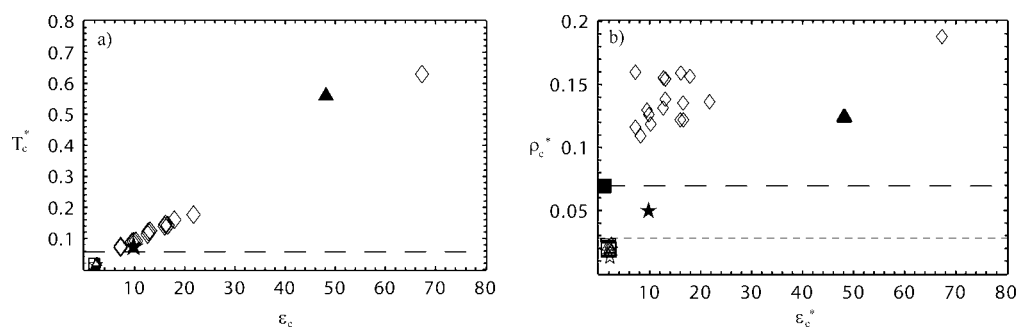


Fig. 6 Critical temperature T_c^* (a) and critical density ρ_c^* (b) of demixing ionic solutions expressed by the RPM variables as function of the dielectric permittivity of the solvent at the CP. The long-dashed line gives the figure of the simulations of the RPM, the short-dashed line is the result of the FL mf theory. Symbols have the same meaning as in previous figures.

If the RPM was adequate, T_c^* should not vary with ϵ . The long-dashed line shows the simulation results. The predicted value of the FL theory for T_c^* is so near to the simulation result that it could not be distinguished on the scale of the plot and, therefore, is not shown. The RPM critical temperatures T_c^* of the various ionic solutions are located on a master curve. We state the almost linear relation between T_c^* and the dielectric constant for the solutions of C_nmimCl in arenes, P_{666 14}Cl and P_{666 14}Br in alkanes, C_nmimBF₄ in alcohols and water, and the systems KI/SO₂ and N₅₅₅₅Br/H₂O. This relation was first suggested in ref. [69] and stated later on for solutions of C_nmim ILs with the anions BF₄ and PF₆ in alcohols [32–34]. For the solutions C₁₂mimCl in arenes, C₁₄mimCl in CCl₄ and P_{666 14}Cl and P_{666 14}Br in alkanes the values of T_c^* and ϵ_c both are very similar so that the systems cannot be distinguished in the plot. The figures of T_c^* for the solutions in long-chain alcohols and KI in SO₂ are close to the RPM value. For the solutions in hydrocarbons, T_c^* is below the RPM value, while the solutions in alcohols with shorter chain length and water yield higher values. On this scale, molecular details of the solvent and of the ILs appear to be unimportant. Minor differences in the critical data for the solutions of the ILs with the BF₄ anion to the findings of others [7,32], which are caused by different amounts of traces of water, cannot be seen on this scale.

The situation for the RPM critical density is ρ_c^* less clear. In Fig. 6b, we draw ρ_c^* as a function of the dielectric constant. We see a tendency that ρ_c^* increases with the dielectric permittivity but the scatter is very large. What can be said is that two groups of data can be identified. For all solutions of alcohols and water, we find a critical density between 0.1–0.2, which is above the figure predicted by the RPM (long-dashed line), while ρ_c^* for the solutions in hydrocarbons is one order of magnitude smaller near to the prediction of the classical FL theory (short-dashed line). The value for the KI/SO₂

solution is between the two groups. It appears that in protic solvents ρ_c^* is above the RPM figure, while for demixing in aprotic solvents smaller figures are found. The distinction in the two sets may be questionable because of the uncertainties about the definition of σ and its estimate. Clearly, an uncertainty of 20 % in σ changes the figure of ρ^* by a factor of two, which, however, is still much smaller than the difference of ρ_c^* observed between solutions in protic and aprotic solvents that is one order of magnitude.

The conjecture of distinct behavior of ionic solutions in protic and aprotic is corroborated by the corresponding-states phase diagrams in the RPM variables $\tau^* = (T^* - T_c^*)/T_c^*$ and $(\rho^* - \rho_c^*)/\rho_c^*$, shown in Fig. 7. One advantage of this representation is that it is independent of the choice of σ . While in the RPM-temperature scale the curvature of the coexistence curves can hardly be seen, it is the purpose of the corresponding-states phase diagram to compare the shapes of coexistence curves. The corresponding-states plot shows clearly that the separation curves of the solutions in water and alcohols appear to have an LCSP, which is a consequence of the decrease of dielectric constant with increasing temperature.

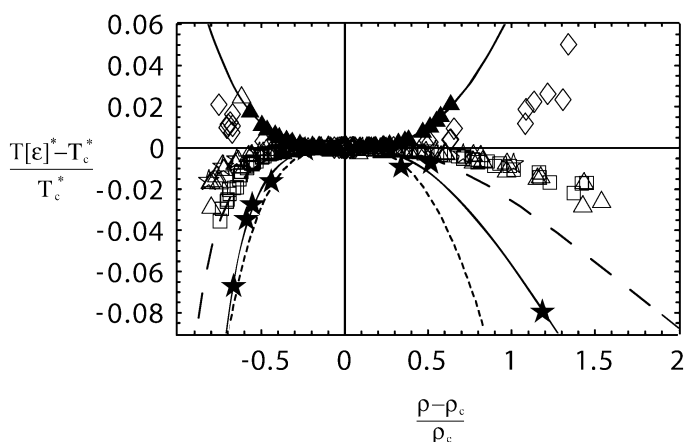


Fig. 7 Corresponding-states phase diagrams for ionic solutions based on the RPM variables. The long-dashed line gives the phase diagram of the RPM, the short-dashed line concerns typical noble gases. Symbols have the same meaning as in previous figures.

This Guggenheim diagram shows that in protic solvents the solutions of ILs have an LCSP, while a UCSP is found for the solutions in aprotic solvents. The drawn curves are the fits to the phase diagrams of the systems KI/SO₂ (filled star) and N₅₅₅Br/H₂O (filled triangle). The figure shows the RPM phase diagram (long-dashed line). The curve is extrapolated from simulation data because the simulations do not reach the near critical region in which the experiments are carried out. The figure also shows the fit to the coexistence curve of noble gases (short-dashed line), taken from Guggenheim's paper [28]. The RPM phase diagram displays a larger width than that of the noble gases and a substantial asymmetry. The width and the asymmetry of the phase diagrams of the IL solutions in hydrocarbons and CCl₄ both appear to be even larger than in the model. Considering the phase diagrams with an LCSP, we see that the width and asymmetry of the IL solutions in alcohols is larger than in N₅₅₅Br/H₂O.

In order to analyze this deviation in more detail, we show in Fig. 8a the widths B^* and in Fig. 8b the diameter slopes A^* of the Guggenheim diagrams in Fig. 7 as functions of ρ_c^* . In order to distinguish the phase diagrams with an LCSP and a UCSP, we have arbitrarily given a negative sign to the parameters of the phase diagrams with LCSP. The dashed line denotes the parameters of the phase diagrams of the noble gases. The filled square gives the parameters obtained from the fit of the simulation data

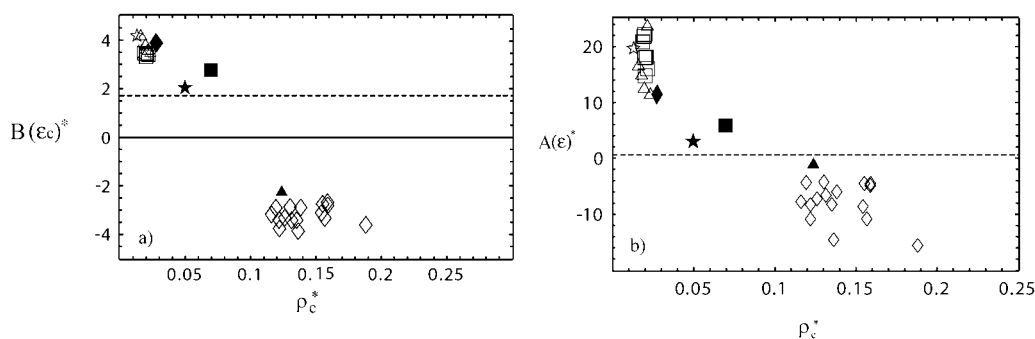


Fig. 8 (a) Width B^* (a) and slope A^* (b) of the diameter of the corresponding-state phase diagrams (see Fig. 7) as functions of the critical density in the RPM scale. The dashed line gives the figure for noble gases. The filled square gives the values obtained from the RPM simulation, and the filled diamond is the result of the FL theory. All other symbols have the same meaning as in previous figures.

of the RPM, and the diamond represents the results of the FL theory, which provides rather realistic estimates for B^* and A^* .

The regions covered by the absolute values of the widths B^* are rather similar for solutions in protic and aprotic solvents. The diameter slopes A^* are larger for the aprotic solvents. In view of the data of the systems KI/SO₂ and N₅₅₅Br, it appears that the absolute values of the parameters A^* and B^* approach the values of the noble gases $A^* = 0.59$ and $B^* = 1.72$, when the dielectric constant of the solvent becomes large. Stronger statements cannot be made at present. There is no correlation with the RPM critical density. Other correlations (e.g., with the dielectric permittivity) could not be found.

DISCUSSION

Considering the huge number of papers concerned with ILs, there is relatively little work on the phase diagrams of solutions and mixtures of ILs. In this work, we have reported and analyzed phase diagrams for the solutions of the ILs C₁₂mimCl in arenes and of C₁₄mimCl in CCl₄ and compared with the phase diagrams of solutions of alkyl phosphonium halides in hydrocarbons [31] and of solutions of C_nmimBF₄ in alcohols and water [32–34,37]. Data taken from the literature on the solutions of KI in SO₂ [43] and of N₅₅₅Br in water [57] were included in the analysis. With the exception of the KI/SO₂ system, all systems considered here have a UCSP. The IL solutions in arenes investigated in this work did not show the LCSP found with other ILs [70,71].

For evaluating the data, a fit function was used that presumes Ising criticality but neglects the non-analytical contributions to the diameter. The fit parameters obtained (critical temperature, critical mole fraction, width of the coexistence curve, and slope of the diameter) allow for an excellent representation of the data. The good quality of the fits can be taken as an argument for the general conclusion that the liquid–liquid phase transitions in ionic solutions belong to the Ising universality class. In a Guggenheim plot showing the reduced temperature $(T - T_c)/T_c$ as a function of the reduced mole fraction $(x^* - x_c^*)/x_c^*$ the phase diagrams of the IL solutions are very similar. The larger width and asymmetry for the solutions in alcohols is noticeable.

In view of the large number of ILs and the even larger number of mixtures which can be prepared, it appears important to search for general trends and basic properties. For this purpose, it is helpful to compare with the properties of simple models. Basic thermodynamic properties of ILs (e.g., the low vapor pressure) are consequences of the Coulomb interactions. Simulations attribute 80 % of the interaction energy to the Coulomb interactions [72]. Therefore, as a first step, the RPM, which considers charged hard spheres of equal size in a dielectric continuum, is taken as a reference model.

Certainly, ILs are anything else but charged hard spheres in a dielectric continuum. However, by expressing the thermodynamic variables in terms of the variables of the RPM, a remarkable result is obtained: with the exception of the solutions in water the data of the CP of solutions of ILs are in the region of the RPM (Fig. 5). Systematic deviations are noticeable that call for an explanation. We draw attention to the almost linear increase of the RPM critical temperature T_c^* with the dielectric constant ϵ of the solvent (Fig. 6a), which includes the solutions in water. The figures for the solutions in the protic solvents are all higher than that of the RPM. At present, there is no theory available explaining this behavior. First simulations of mixtures of charged hard spheres and dipolar hard spheres seem to show the trend just described [73].

For the critical density ρ_c^* no clear correlation with ϵ , or any other property, could be found. Scaling the number density by the molecular volume did not give a clearer picture. However, the two groups of solutions in protic and aprotic solvents can clearly be distinguished. In solutions in protic solvents, such as alcohols and water, ρ_c^* is higher than expected for the RPM, while in solutions in aprotic solvents ρ_c^* is lower. Remarkably, in the RPM variables the CPs of the solutions of the ILs in arenes and hydrocarbons can hardly be distinguished, although rather different ILs are considered. This observation may be taken as an argument for our choice of the charge separation at close contact as the relevant distance to be used when transforming the thermodynamic variables into the dimensionless RPM variables.

The corresponding-state phase diagram in terms of the RPM variables provides a spectacular distinction between the solutions in protic and aprotic solvents. Taking into account that the dielectric permittivity ϵ of the solvents depends on the temperature (which was not done in former work) it is found that in protic solvents the CP becomes an LCSP, while in aprotic solvents all systems show a UCSP. With decreasing temperature, the dielectric constant ϵ of alcohols and water is enhanced, which causes an increase of the RPM temperature with decreasing temperature. As a consequence, the UCSP in the normal temperature scale becomes an LCSP in the RPM scale. It appears that the strengthening of the hydrogen bonds in alcohols and water with decreasing temperature gives a contribution to the driving force of the liquid–liquid phase transition in protic solvents. For the solutions in alkanes, alkenes, and CCl_4 , the temperature dependence of ϵ is unimportant; thus, the CP remains a UCSP. In polar aprotic solvents, the decrease of the dielectric constant with increasing temperature lowers the RPM temperature. As a consequence, the LCSP of KI/SO_2 becomes a UCSP in the RPM variables, which is expected for Coulomb systems. The finding is in accordance with a report on a solution of N_{1112}Br in chloroform [74], where experiments yielded an LCSP that, after rescaling in the RPM variables, also became a UCSP.

The analysis of the Guggenheim plots based on the phase diagrams in RPM variables yields no substantial difference between the absolute values of the widths B^* for the solutions in protic and aprotic solvents. The figures scatter about the value obtained from the simulations of the RPM, which, as is well known, is larger than that of nonpolar fluids. Similarly, the slope of the diameter A^* observed for the solutions of the ILs is in the region predicted for the RPM. The figures for the solutions in aprotic solvents appear larger than those for protic solvents. The estimates of the width and the diameter slope resulting from the classical FL theory are in remarkably good agreement with the experimental results for the solutions in aprotic solvents, which may be somewhat fortuitous. For both properties B^* and A^* , it appears that the figures of the nonpolar gases are approached with increasing dielectric permittivity of the solvent.

We recall that the fit assuming the rectilinear diameter is an approximation, which is appropriate in view of the limited accuracy of the present measurements. Measurements appropriate for analyzing the nonanalytic contributions to the diameter of the coexistence curves in demixing ionic solutions that will allow an adequate characterization of the asymmetry of the phase diagrams are underway.

CONCLUSIONS

Phase diagrams of the liquid–liquid phase transition in ionic solutions are consistent with Ising critical behavior as are the phase transitions of nonionic systems. The CPs in ionic solutions are in the region which is expected for the model system of charged hard spheres (RPM). The analysis of the phase diagrams in terms of the RPM variables, however, shows systematic deviations for various properties. The critical temperature shows an essentially linear correlation with the dielectric constant, where the solutions in protic solvents (including water) show figures above that of the RPM, while the critical temperatures in solutions in aprotic solvents are below this value. Similarly, the critical densities for solutions in protic solvents are above and in aprotic solvents below the RPM value. Using RPM variables, the shapes of the coexistence curves of the solutions in aprotic and protic solvents are qualitatively different. In aprotic solvents, we find a UCSP and an LCSP in protic solvents. It appears that the strengthening of the hydrogen bonds in protic solvents with decreasing temperature gives a contribution to the driving force of the phase transition. The absolute width of the phase diagrams is similar for the solutions in protic and aprotic solvents, while the slope of the diameter appears to be larger in aprotic solvents. These conclusions are based on a substantial body of experimental observations and call for explanations by theory and simulations.

ACKNOWLEDGMENTS

The work was supported by the grant SCHR188/10-1 of the Deutsche Forschungsgemeinschaft in the SSP “Ionic Liquids”. Inspiring discussions with Profs. M. A. Anisimov and H. Weingärtner are acknowledged.

REFERENCES

1. R. D. Rogers, K. R. Seddon (Eds.). *Ionic Liquids: Industrial Applications for Green Chemistry*, ACS Symposium Series No. 818, American Chemical Society, Washington, DC (2002).
2. R. D. Rogers, K. R. Seddon (Eds.). *Ionic Liquids as Green Solvents: Progress and Prospects*, ACS Symposium No. 856, American Chemical Society, Washington, DC (2003).
3. P. Wasserscheid, W. Keim. *Angew. Chem., Int. Ed.* **39**, 3772 (2000).
4. J. D. Holbrey, K. R. Seddon. *J. Chem. Soc., Dalton Trans.* 2133 (1999).
5. D. H. Zaitsau, G. J. Kabo, A. A. Strechan, Y. U. Paulecka, A. Tschersich, S. V. Verevkin, A. Heintz. *J. Phys. Chem. A* **110**, 7303 (2006).
6. L. P. Rebelo, J. N. Canognia Lopes, J. M. S. S. Esperanca, E. Filipe. *J. Phys. Chem. B* **109**, 6040 (2005).
7. D. H. Zaitsau, Y. U. Paulechka, G. J. Kabo. *J. Phys. Chem. A* **110**, 11602 (2006).
8. K. S. Pitzer. *J. Phys. Chem.* **99**, 13070 (1995).
9. M. A. Anisimov. *Critical Phenomena in Liquids and Liquid Crystals*, Gordon and Breach, Philadelphia (1991).
10. R. F. Kayser, H. J. Raveche. *Phys. Rev. A* **29**, 1013 (1984).
11. R. R. Singh, K. S. Pitzer. *J. Chem. Phys.* **92**, 6775 (1990).
12. K. C. Zhang, M. E. Briggs, R. W. Gammon, J. M. H. Levelt Sengers. *J. Chem. Phys.* **97**, 8692 (1992).
13. S. Wiegand, M. E. Briggs, J. M. H. Levelt Sengers, M. Kleemeier, W. Schröer. *J. Chem. Phys.* **109**, 9038 (1998).
14. M. Kleemeier, S. Wiegand, W. Schröer, H. Weingärtner. *J. Chem. Phys.* **110**, 3085 (1999).
15. G. Orkoulas, A. Z. Panagiotopoulos. *J. Chem. Phys.* **110**, 1581 (1999).
16. A. Z. Panagiotopoulos. *J. Chem. Phys.* **116**, 3007 (2002).
17. G. Orkoulas, A. Z. Panagiotopoulos, M. E. Fisher. *Phys. Rev. E* **61**, 5930 (2000).

18. J.-M. Caillol, D. Levesque, J.-J. Weiss. *J. Chem. Phys.* **116**, 10794 (2002).
19. Q. L. Yan, J. J. de Pablo. *J. Chem. Phys.* **111**, 9509 (1999).
20. Q. L. Yan, J. J. de Pablo. *Phys. Rev. Lett.* **88**, 095504 (2002).
21. J. M. Romero-Enrique, G. Orkoulas, A. Z. Panagiotopoulos, M. E. Fisher. *Phys. Rev. Lett.* **85**, 4558 (2000).
22. H. Weingärtner, W. Schröer. *Adv. Chem. Phys.* **116**, 1 (2001).
23. W. Schröer, M. Wagner, O. Stanga. *J. Mol. Liq.* **127**, 2 (2006).
24. M. A. Anisimov, J. V. Sengers. "The critical region", in *Equations of State for Fluids and Fluid Mixtures*, J. V. Sengers, R. F. Kayser, C. J. Peters, H. J. White (Eds.), Elsevier, Amsterdam (2000).
25. J. Wang, M. A. Anisimov. *Phys. Rev. E* **75**, 051107 (2007).
26. C. A. Cerdeirina, M. A. Anisimov, J. V. Sengers. *Chem. Phys. Lett.* **424**, 414 (2006).
27. J. O. Hirschfelder, C. F. Curtis, R. B. Bird. *Molecular Theory of Gases and Liquids*, John Wiley, New York (1964).
28. E. A. Guggenheim. *J. Chem. Phys.* **13**, 253 (1945).
29. V. C. Weiss, W. Schröer. *J. Chem. Phys.* **122**, 084705 (2005).
30. H. Weingärtner, T. Merkel, U. Maurer, J.-P. Conzen, H. Glasbrenner, S. Käshammer. *Ber. Bunsen-Ges. Phys. Chem.* **95**, 1579 (1991).
31. D. Saracsan, C. Rybarsch, W. Schröer. *Z. Phys. Chem.* **220**, 1417 (2006).
32. M. Wagner, O. Stanga, W. Schröer. *Phys. Chem. Chem. Phys.* **5**, 3943 (2003).
33. M. Wagner, O. Stanga, W. Schröer. *Phys. Chem. Chem. Phys.* **6**, 4421 (2004).
34. W. Schröer. *J. Mol. Liq.* **125**, 164 (2006).
35. K. N. Marsh, A. Deev, C.-T. Wu, E. Tran, A. Klamt. *Kor. J. Chem. Eng.* **19**, 357 (2002).
36. C.-T. Wu, K. N. Marsh, A. V. Deev, J. A. Boxall. *J. Chem. Eng. Data* **48**, 486 (2003).
37. J. M. Crosthwaite, S. N. V. K. Aki, E. J. Maginn, J. F. Brennecke. *J. Phys. Chem. B* **108**, 5113 (2004).
38. A. Heintz, J. Lehmann, C. Wertz. *J. Chem. Eng. Data* **48**, 472 (2003).
39. A. Shariati, C. J. Peters. *J. Supercrit. Fluids* **25**, 109 (2003).
40. A. Shariati, C. J. Peters. *J. Supercrit. Fluids* **30**, 139 (2004).
41. J. Lachwa, J. Szydłowski, V. Naidanovic-Visac, L. R. N. Rebelo, K. R. Seddon, M. Nunes da Ponte, J. M. S. S. Esperanca, H. J. R. Guedes. *J. Am. Chem. Soc.* **127**, 6542 (2005).
42. U. Domanska, L. M. Casas. *J. Phys. Chem. B* **111**, 4109 (2007).
43. P. Walden, M. Centnerszwer. *Z. Phys. Chem.* **42**, 432 (1903).
44. M. Ley-Koo, M. S. Green. *Phys. Rev. A* **23**, 2650 (1981).
45. A. Kumar, H. R. Krishnamurthy, E. S. R. Gopal. *Phys. Rep.* **98**, 57 (1983).
46. S. C. Greer, B. K. Das, A. Kumar, E. S. R. Gopal. *J. Chem. Phys.* **79**, 4554 (1983).
47. M. A. Anisimov, E. E. Gorodetskii, V. D. Kulikov, J. V. Sengers. *Phys. Rev. E* **51**, 1199 (1995).
48. Y. C. Kim, M. E. Fisher, G. Orkoulas. *Phys. Rev. E* **67**, 061506 (2003).
49. J. M. Prausnitz, R. N. Lichtenthaler, E. Gomes de Azevedo. *Molecular Thermodynamics of Fluid-Phase Equilibria*, 2nd ed., Prentice-Hall, Englewood Cliffs (1989).
50. A. Z. Panagiotopoulos. *Fluid Phase Equilib.* **76**, 97 (1992).
51. J. M. Caillol. *J. Chem. Phys.* **100**, 2161 (1994).
52. G. Orkoulas, A. Z. Panagiotopoulos. *J. Chem. Phys.* **101**, 1452 (1994).
53. M. E. Fisher, Y. Levin. *Phys. Rev. Lett.* **71**, 3826 (1993).
54. Y. Levin, M. E. Fisher. *Physica A* **225**, 164 (1996).
55. P. Debye, E. Hückel. *Physik. Z* **24**, 185 (1923).
56. J. V. Sengers, J. M. H. Levelt Sengers. In *Progress in Liquid Physics*, C. A. Croxton (Ed.), John Wiley, New York (1978).
57. M. L. Japas, J. M. H. Levelt Sengers. *J. Phys. Chem.* **94**, 5361 (1990).
58. J. M. S. Esperanca, H. J. R. Guedes, M. Blesic, L. P. N. Rebelo. *J. Chem. Eng. Data* **51**, 237 (2006).

59. C. P. Fredlake, J. M. Crostwaite, D. G. Hert, S. N. V. K. Aki, J. F. Brennecke. *J. Chem. Eng. Data* **49**, 954 (2004).
60. C. J. Bradaric, A. Downard, C. Kennedy, A. J. Robertson, Y. Zhou. *Green Chem.* **5**, 143 (2003).
61. *Handbook of Chemistry and Physics*, 49th ed., Chemical Rubber, Cleveland (1968).
62. Landolt Börnstein New Series IV/8, Springer, Berlin (1996).
63. A. L. Horwath (Ed). *Physical Properties of Inorganic Compounds*, Arnold, London (1975).
64. Landolt Börnstein New Series IV/6, Springer, Berlin (1991).
65. *Tables of Interatomic Distances and Configuration in Molecules and Ions*, The Chemical Society, London (1958).
66. A. J. Arduengo III, H. V. R. Dias, R. L. Harlow, M. Kline. *J. Am. Chem. Soc.* **114**, 5530 (1992).
67. C. Hardacre, J. D. Holbrey, S. E. J. McMath, D. T. Bowro, A. K. Soper. *J. Chem. Phys.* **118**, 273 (2003).
68. D. J. Abdallah, R. E. Bachman, J. Perlstein, R. C. Weiss. *J. Phys. Chem. B* **103**, 9269 (1999).
69. W. Schröer, H. Weingärtner. *Pure Appl. Chem.* **76**, 19 (2004).
70. J. Lachwa, I. Bento, M. T. Duarte, J. N. Canonica Lopes, L. P. N. Rebelo. *Chem. Commun.* 2445 (2006).
71. J. Lachwa, J. Szydłowski, V. Najdanovic-Visak, A. Makovska, K. R. Seddon, J. M. S. S. Esperanca, H. J. R. Guedes, L. P. N. Rebelo. *Green Chem.* **8**, 262 (2006).
72. C. G. Hanke, S. L. Price, R. M. Lynden-Bell. *Mol. Phys.* **99**, 801 (2001).
73. J. C. Shelley, G. N. Patey. *J. Chem. Phys.* **110**, 1633 (1999).
74. S. Wiegand, M. Kleemeier, J. M. Schröder, W. Schröer, H. Weingärtner. *Int. J. Thermophys.* **15**, 1045 (1994).